Supplementary materials

Selective addition of ferric hydroxide to Feammox nitrogen transformation favors vivianite formation for phosphorus removal

Xiaohui Cheng[1], Lanlan Hu[1], Xiaotong Cen[2], Tao Liu,[3] Xiang Cheng[1], Kangning Xu[1,*], Min Zheng[2,*]

[1]Beijing Key Lab for Source Control Technology of Water Pollution, College of Environmental Science and Engineering, Beijing Forestry University, Beijing 100083, China

[2]Water Research Centre, School of Civil and Environmental Engineering, University of New South Wales, Sydney, New South Wales 2052, Australia

[3]Department of Civil and Environmental Engineering, The Hong Kong Polytechnic University, Hong Kong 999077, China

***Corresponding authors**

Email address: xukangning@bjfu.edu.cn (K.X); min.zheng1@unsw.edu.au (M.Z)

Number of texts: 1

Number of tables: 1

Number of figures: 6

Text S1. Procedure of sequential phosphorus extraction analysis

Phosphorus species bound in minerals in the sludge were analyzed using sequential phosphate extraction methods. The 2,2'-bipyridine + KCl and bicarbonate dithionite (BD) extractions were used to quantify phosphate bound in vivianite (Bipy-P) and with reducible metals (e.g., Fe(III)) (BD-P), respectively, following the methods described by Gu et al. (2016) and Wang et al. (2021). In brief, the samples were oscillated with 25 mL mixture solution of 0.2 % bipyridine and 0.1 M KCl at 50 °C for 24 h. The suspension was filtered by 0.45 μm filter membrane and an extraction solution in red was obtained. 1 mL of the extraction solution was then added into 10 mL colorimetric tube with 0.2 mL 2 M H_2SO_4 and 8.8 mL deionized water. When the solution became colorless, the phosphorus content in vivianite was measured according to molybdenum antimony anti-spectrophotometry methods. The remaining extraction solution from the previous step was incubated in 25 mL 0.11 M BD solution and shaken for 1 h to extract BD-P. Notably, the bipyridine solution does not require N_2 purging, as Fe(II) oxidation is inhibited by the binding of bipyridine to the sample surface.

Table S1. Summary of research results on Feammox activity in different habitats reported in previous studies, including natural wetlands, farmland soils, lake catchments, constructed wetlands, and batch or bioreactors.

Sampling environments		Feammox-related microbes	Reference
Natural wetlands	Intertidal wetland	*Geobacteraceae*,	(Li et al., 2015)
	Riparian zone	*Anaeromyxobacter*, *Pseudomonas*, *Geobacter*	(Ding et al., 2017)
	Yellow River wetland	*Anaeromyxobacter*, *Geobacter*	(Guan et al., 2023)
Farmland soils	Paddy soil	*Geobacter*, *Desulfovibrio*, *Clostridium*, *Pseudomonas*	(Zhou et al., 2016)
	Paddy soil	*Geobacter*, *Pseudomonas*	(Li et al., 2019)
	Wheat-rice rotation area	*Bacillus*, *Geobacter*, *Anaeromyxobacter*	(Qin et al., 2019)
	Farmland soils	*Geobacter*, *Anaeromyxobacter*, *Pseudomonas*, *Thiobacillus*, *Bacillus*	(Ding et al., 2020a)
	Paddy soil	*Bacillus*, *Anaeromyxobacter, Pseudomonas*, *Geobacter*	(Ding et al., 2021)
	Farmland soil	*Sphingomonas*, *Clostridium*	(Ma et al., 2021)
	Farmland soil	*Geobacteraceae*	(Ding et al., 2022)
	Paddy soils	*Geobacter*, *Anaeromyxobacter*, *Clostridium*	(Ma et al., 2024)
	Soil or sediment samples	*Pseudomonas*, *Rhodanobacter*, *Acinetobacter*, *Thermomonas*	(Ma et al., 2022)
Lake catchments	Taihu estuary region	*Geobacter*, *Anaeromyxobacter*, *Pseudomonas*	(Ding et al., 2019)
	Taihu watershed	*Geobacter*, *Anaeromyxobacter*	(Ding et al., 2020b)
	Eutrophic lake	*Geobacteraceae*	(Yao et al., 2019)
	Shallow freshwater lake	*Geobacteraceae*	(Yao et al., 2020)
Constructed wetlands	Wetland-microbial fuel cell	*Geobacter*	(Yang et al., 2021)
	Iron-carbon micro-electrolysis constructed wetlands	*Pseudomonas*	(Zheng et al., 2023)

Batch or bioreactors	Anaerobic microbial culture tank	*Pseudomonas*, *Geobacter*	(Li et al., 2018)
	Multistage Feammox Bioreactor	*Pseudomonas*, *Geobacter*	(Nguyen et al., 2023)
	Electrochemically assisted Feammox system	*Geobacter*, *Clostridium*, *Achromobacter*, *Thermomonas*, *Pseudomonas*, *Thiobacillus*	(Wang et al., 2024)
	Hollow fiber membrane bioreactors	*Geobacter*	(Cerda et al., 2024)
	Iron-mediated anoxic-microaerobic (A/O) process	*Ignavibacterium, Geobacter*	(Xu et al., 2024)

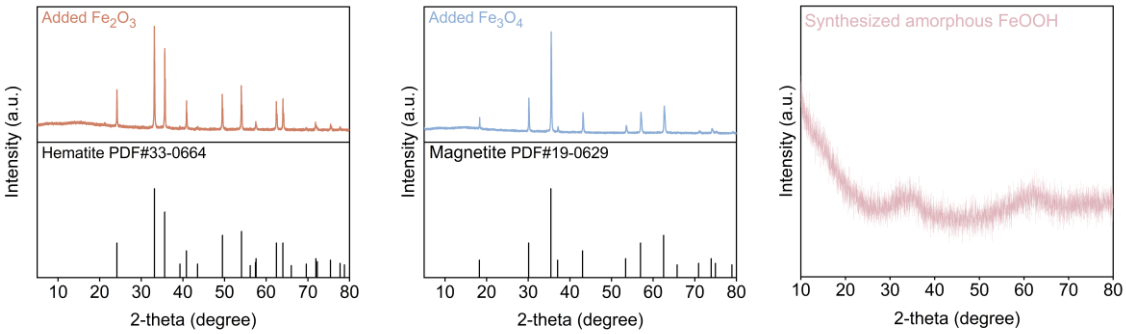

Fig. S1. XRD patterns of α-Fe_2O_3, Fe_3O_4 and synthesized amorphous FeOOH.

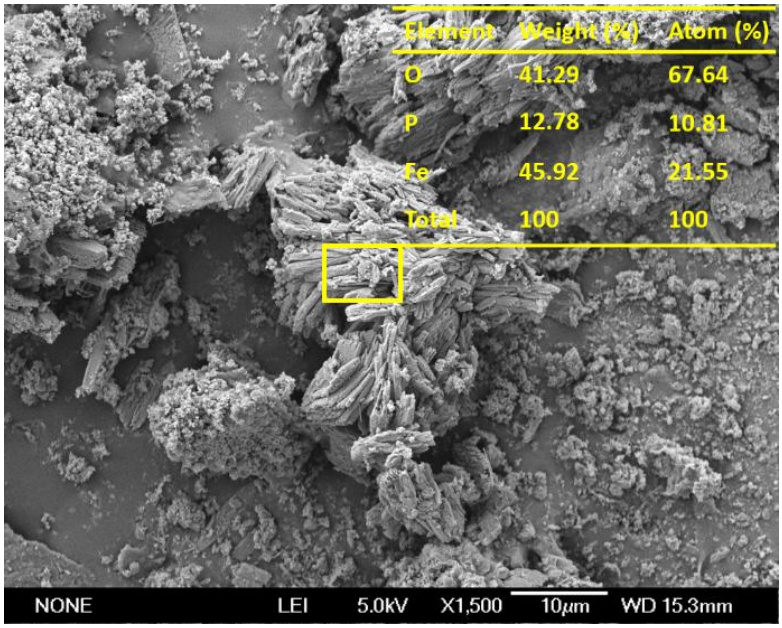

Fig. S2. SEM and EDS results of the solid products.

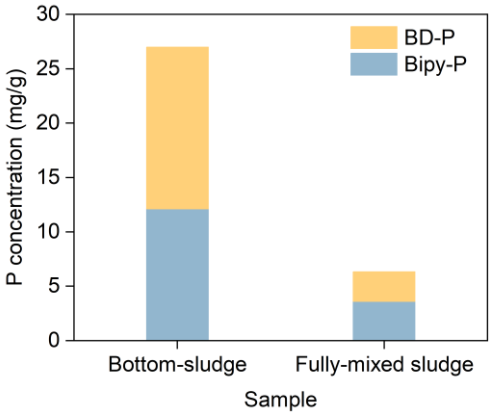

Fig. S3. Different phosphate fractions bound in iron minerals in the bottom sludge and the fully-mixed sludge collected on day 310. Bipy-P is phosphate bound in vivianite "$Fe_3(PO_4)_2 \cdot 8H_2O$", and BD-P represents phosphate bound in oxidized vivianite, ferric phosphate and other Fe(III) compounds like amorphous FeOOH. The proportions of Bipy-P and BD-P in the fully-mixed sludge were consistent with the results obtained using the bottom sludge. The concentrations of Fe(II)- and Fe(III)-vivianite in the bottom sludge were significantly higher than those in the fully-mixed sludge. As known, the density of vivianite crystals of 2.68 g/cm^3 is much higher than the approximate density of sludge at 1 g/cm^3. As a result, vivianite crystals preferred to settle at the bottom of the bioreactor.

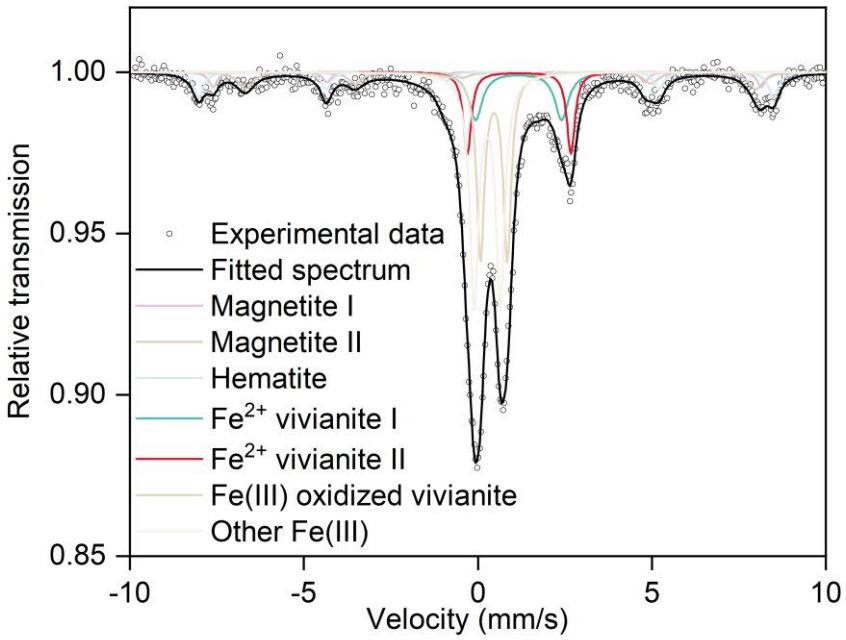

Fig. S4. Mössbauer spectra of the sludge sample collected from the bioreactor on day 310.

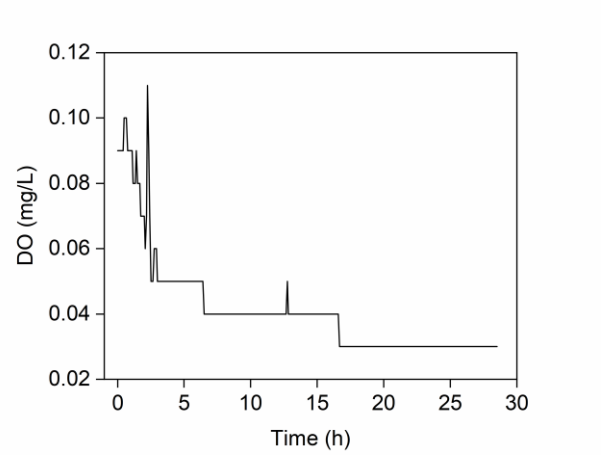

Fig. S5. Changes of the DO concentrations in bioreactor taking the measurement on day 120 as an example. The fluctuations in DO concentrations during the first 2 hours were likely due to the installation of the DO sensor. After stabilization, the DO concentration decreased by less than 0.06 mg/L, indicating a consistently low DO level in the bioreactor.

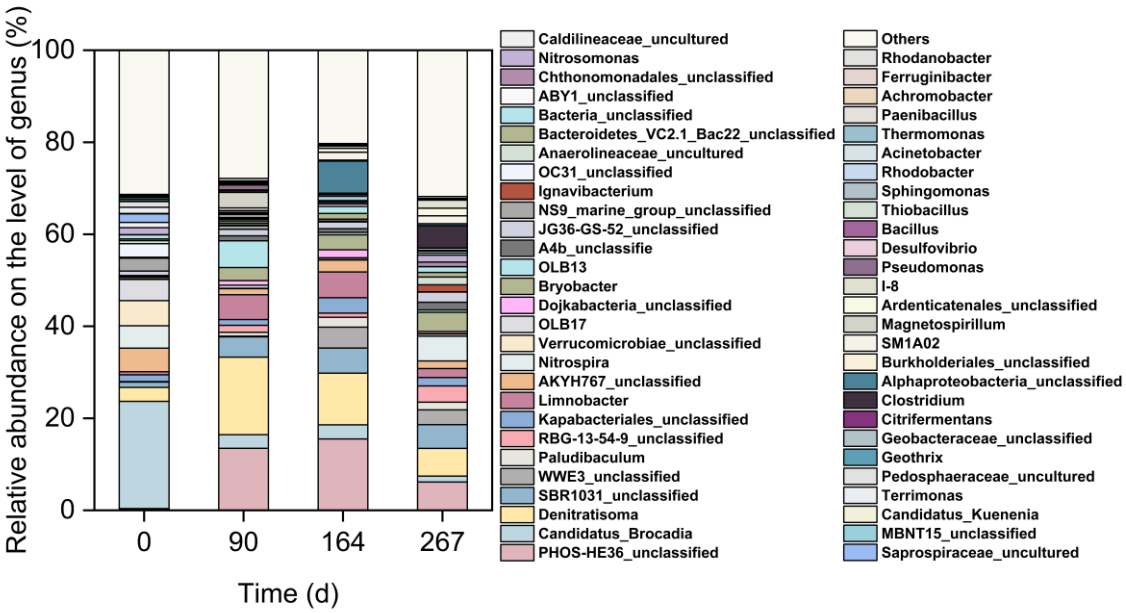

Fig. S6. Relative abundances of bacteria at genus level in the sludge samples collected from the bioreactor on days 0, 90, 164, and 267.

References

Cerda, Á., Rodríguez, C., González, M., González, H., Serrano, J. and Leiva, E., 2024. Feammox bacterial biofilm formation in HFMB. Chemosphere. 358, 142072.

Ding, B., Chen, Z., Li, Z., Qin, Y. and Chen, S., 2019. Nitrogen loss through anaerobic ammonium oxidation coupled to Iron reduction from ecosystem habitats in the Taihu estuary region. Sci. Total Environ. 662, 600-606.

Ding, B., Li, Z., Cai, M., Lu, M. and Liu, W., 2022. Feammox is more important than anammox in anaerobic ammonium loss in farmland soils around Lake Taihu, China. Chemosphere. 305, 135412.

Ding, B., Li, Z. and Qin, Y., 2017. Nitrogen loss from anaerobic ammonium oxidation coupled to Iron(III) reduction in a riparian zone. Environ. Pollut. 231, 379-386.

Ding, B., Luo, W., Qin, Y. and Li, Z., 2020a. Effects of the addition of nitrogen and phosphorus on anaerobic ammonium oxidation coupled with iron reduction (Feammox) in the farmland soils. Sci. Total Environ. 737, 139849.

Ding, B., Qin, Y., Luo, W. and Li, Z., 2020b. Spatial and seasonal distributions of Feammox from ecosystem habitats in the Wanshan region of the Taihu watershed, China. Chemosphere. 239, 124742.

Ding, B., Zhang, H., Luo, W., Sun, S., Cheng, F. and Li, Z., 2021. Nitrogen loss through denitrification, anammox and Feammox in a paddy soil. Sci. Total Environ. 773, 145601.

Gu, S., Qian, Y., Jiao, Y., Li, Q., Pinay, G. and Gruau, G., 2016. An innovative approach for sequential extraction of phosphorus in sediments: Ferrous iron P as an independent P fraction. Water Res. 103, 352-361.

Guan, Q., Li, T., Zhou, Y., Yang, F. and Li, Q., 2023. Evidence of nitrogen loss from anaerobic ammonium oxidation coupled with ferric iron reduction in the Yellow River wetland. EGUsphere. 2023, 1-36.

Li, H., Su, J., Yang, X., Zhou, G., Lassen, S.B. and Zhu, Y., 2019. RNA stable isotope probing of potential Feammox population in paddy soil. Environ. Sci. Technol. 53 (9), 4841-4849.

Li, X., Hou, L., Liu, M., Zheng, Y., Yin, G., Lin, X., Cheng, L., Li, Y. and Hu, X., 2015. Evidence of nitrogen loss from anaerobic ammonium oxidation coupled with ferric iron reduction in an intertidal wetland. Environ. Sci. Technol. 49 (19), 11560-11568.

Li, X., Yuan, Y., Huang, Y., Liu, H.-w., Bi, Z., Yuan, Y. and Yang, P.-b., 2018. A novel method of simultaneous NH_4^+ and NO_3^- removal using Fe cycling as a catalyst: Feammox coupled with NAFO. Sci. Total Environ. 631-632, 153-157.

Ma, D., Wang, J., Fang, J., Jiang, Y. and Yue, Z., 2024. Asynchronous characteristics of Feammox and iron reduction from paddy soils in Southern China. Environ. Res. 252, 118843.

Ma, D., Wang, J., Li, H., Che, J. and Yue, Z., 2022. Simultaneous removal of COD and NH_4^+-N from domestic sewage by a single-stage up-flow anaerobic biological filter based on Feammox. Environ. Pollut. 314, 120213.

Ma, D., Wang, J., Xue, J., Yue, Z., Xia, S., Song, L. and Gao, H., 2021. Effects of soil pH on gaseous nitrogen loss pathway via Feammox process. Sustainability. 13 (18), 1-11.

Nguyen, H.T., Nguyen, L.D., Le, C.P., Hoang, N.D. and Dinh, H.T., 2023. Nitrogen and carbon removal from anaerobic digester effluents with low carbon to nitrogen ratios under Feammox conditions. Bioresour. Technol. 371, 128585.

Qin, Y., Ding, B., Li, Z. and Chen, S., 2019. Variation of Feammox following ammonium fertilizer migration in a wheat-rice rotation area, Taihu Lake, China. Environ. Pollut. 252, 119-127.
Wang, Q., Kim, T.-H., Reitzel, K., Almind-Jørgensen, N. and Nielsen, U.G., 2021. Quantitative determination of vivianite in sewage sludge by a phosphate extraction protocol validated by PXRD, SEM-EDS, and ^{31}P NMR spectroscopy towards efficient vivianite recovery. Water Res. 202, 117411.
Wang, T., Zhang, J., Wang, Z., Zhao, Q., Wu, Y., Li, N., Jiang, X. and Wang, X., 2024. Bioelectrochemically enhanced autotrophic Feammox for ammonium removal via the Fe(II)/Fe(III) cycle. Environ. Sci.: Water Res. Technol. 10 (6), 1355-1364.
Xu, H., Zhang, L., Li, Z., Chen, Y., Yang, B. and Zhou, Y., 2024. Activation of iron oxides through organic matter-induced dissolved oxygen penetration depth dynamics enhances iron-cycling driven ammonium oxidation in microaerobic granular sludge. Water Res. 266, 122400.
Yang, Y., Zhao, Y., Tang, C., Mao, Y., Chen, T. and Hu, Y., 2021. Novel pyrrhotite and alum sludge as substrates in a two-tiered constructed wetland-microbial fuel cell. J. Clean Prod. 293, 126087.
Yao, Z., Wang, F., Wang, C., Xu, H. and Jiang, H., 2019. Anaerobic ammonium oxidation coupled to ferric iron reduction in the sediment of a eutrophic lake. Environmental Science and Pollution Research. 26 (15), 15084-15094.
Yao, Z., Yang, L., Song, N., Wang, C. and Jiang, H., 2020. Effect of organic matter derived from algae and macrophyte on anaerobic ammonium oxidation coupled to ferric iron reduction in the sediment of a shallow freshwater lake. Environ. Sci. Pollut. Res. 27 (21), 25899-25907.
Zheng, X., Zhou, C., Wu, F., Xu, H., Zhao, Z., Han, Z., Zhang, H. and Yang, S., 2023. Enhanced removal of organic, nutrients, and PFCs in the iron-carbon micro-electrolysis constructed wetlands: Mechanism and iron cycle. Chem. Eng. J. 457, 141174.
Zhou, G., Yang, X., Li, H., Marshall, C.W., Zheng, B., Yan, Y., Su, J. and Zhu, Y., 2016. Electron shuttles enhance anaerobic ammonium oxidation coupled to iron(III) reduction. Environ. Sci. Technol. 50 (17), 9298-9307.